Non-Orthogonal Domain Parabolic Equation and Its Tilted Gaussian Beam Solutions

Yakir Hadad and Timor Melamed

***Abstract*—A non-orthogonal coordinate system which is *a priori* matched to localized initial field distributions for time-harmonic wave propagation is presented. Applying, in addition, a rigorous paraxial-asymptotic approximation, results in a novel parabolic wave equation for beam-type field propagation in 3D homogeneous media. Localized solutions to this equation that exactly match linearly-phased Gaussian aperture distributions are termed tilted Gaussian beams. These beams serve as the building blocks for various beam-type expansion schemes. Application of the scalar waveobjects to electromagnetic field beam-type expansion, as well as reflection and transmission of these waveobjects by planar velocity (dielectric) discontinuity are presented. A numerical example which demonstrates the enhanced accuracy of the tilted Gaussian beams over the conventional ones concludes the paper.**

***Index Terms*—Electromagnetic propagation, electromagnetic theory, Gaussian beams, propagation.**

I. Introduction and Statement of the Problem

THE parabolic wave equation (PWE) models propagation of linear waves which is predominant in one direction. In this paper we refer to this direction as the "paraxial direction." Under this assumption, as well as other asymptotic considerations, the Helmholtz equation is reduced to a much simpler form of a PWE [1]–[3]. Solutions of the PWE are subject to boundary conditions which are obtained by matching the field initial distribution on a given surface to the PWE near-field model. For problems in which the aperture distribution is given over a surface that is transverse to the initial paraxial direction, it may be conveniently matched to the PWE. Thus the field can be propagated in a step-by-step manner, by evaluating the field in each step from its distribution in the previous one.

The concept of PWE was first introduced with relation to radio propagation over realistic earth surfaces [4], followed by its generalization which combined it with the well-known ray coordinates of geometric optics that resulted in a new diffraction theory [5]. Mathematical refinements and further developments of the PWE method have been achieved in [6]–[11], along with some more recent work [12]–[17].

Important solutions of the PWE include its different beam-type waveobjects [18]–[23]. PWE methods may also be utilized for solving beam-type waveobjects propagation in generic media profiles such as inhomogeneous [24]–[26], anisotropic [27]–[31], and time-dependent pulsed beams in dispersive media [32]–[36]. The need for these solutions arises from beam-type expansions such as Gabor-based expansions [37], [38] or the frame-based field expansion [39], [40]. The latter utilizes the key feature of the beam's continuous spectrum [38], [41], [42], and discretized the spectral representation with no loss of essential data for reconstruction. A theoretical overview of frame-based representation of scalar time-harmonic fields was presented in [39], with an extension to electromagnetic fields in [43], and for time-dependent scalar fields in [40].

Exact beam-type expansions require beam solutions that match localized aperture planar distributions. In these solutions, as well as in other different propagation scenarios, the boundary plane over which the initial field distribution is given is generally *not perpendicular* to the paraxial direction of propagation. Therefore, in order to use conventional (orthogonal coordinates) Gaussian beams, apart from asymptotic approximations, an additional approximation is carried out to project the initial field complex curvature matrix on a plane *normal* to the beam axis direction. This additional approximation reduces the accuracy of the resulting beam solutions especially for large angle departures and, moreover, it becomes *inconsistent with respect to asymptotic orders*. The need for the additional approximation may be avoided by applying a *non-orthogonal coordinates system*. This work is concerned with obtaining a novel form of PWE in non-orthogonal coordinates such that its beam-type solutions are matched *exactly* to linearly-phased Gaussian distributions over a tilted plane with respect to the beam-axis.

We seek for *asymptotically-exact* Gaussian beam (GB) solutions $\widehat{B}(\mathbf{r})$, to the 3D scalar Helmholtz equation

$$[\nabla^2 + k^2]\widehat{B}(\mathbf{r}) = 0, \quad \nabla^2 = \frac{\partial^2}{\partial x_1^2} + \frac{\partial^2}{\partial x_2^2} + \frac{\partial^2}{\partial z^2} \qquad (1)$$

in the $z \geq 0$ half-space, where $k = \omega/v_0$ is the homogeneous medium wavenumber with v_o being the medium wave-speed and $\widehat{B}(\mathbf{r})$ a time-harmonic scalar field with suppressed time-dependence of $\exp(j\omega t)$. In (1), $\mathbf{r} = (x_1, x_2, z)$ is the conventional Cartesian coordinate frame with $\mathbf{x} = (x_1, x_2)$ denoting the transverse coordinates (see Fig. 1). Another objective is to obtain GB which can serve as the building blocks for beam-type expansion schemes of scalar [39], as well as electromagnetic [43] fields. These expansion schemes decompose the field over a spatial-directional (spectral) lattice according to spatial and directional spectral variables (see (37)). The propagating elements

Manuscript received April 05, 2009; revised September 29, 2009; accepted October 22, 2009. Date of publication January 26, 2010; date of current version April 07, 2010.

The authors are with the Department of Electrical and Computer Engineering, Ben-Gurion University of the Negev, Beer Sheva 84105, Israel (e-mail: timormel@ee.bgu.ac.il).

Digital Object Identifier 10.1109/TAP.2010.2041161

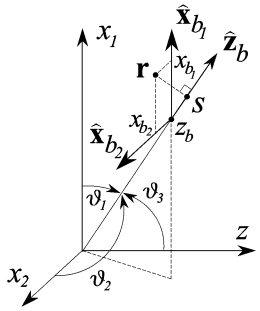

Fig. 1. Non-orthogonal local beam coordinate system. Observation point $\mathbf{r} = (x_{b_1}, x_{b_1}, z_b)$ where z_b is the origin location along the paraxial propagation direction, $\hat{\mathbf{z}}_b$, and the transverse coordinates, x_{b_1} and x_{b_1}, lie on a plane parallel to the (x_1, x_2) plane. Thus, the transverse coordinates are tilted with respect to the propagation direction z_b. The phase term in (13) is accumulated according to the (perpendicular) optic length (Eikonal) s.

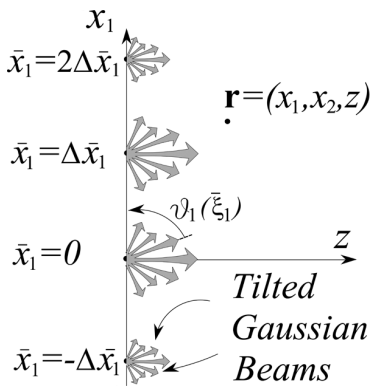

Fig. 2. The fields in $z \geq 0$ are evaluated by a superposition of shifted tilted EM GB propagators which emanate from the initial distribution plane over the discrete spatial-directional lattice in (37). Each beam propagator emanates from a lattice point $(\bar{x}_1, \bar{x}_1) = (m_1 \Delta \bar{x}_1, m_2 \Delta \bar{x}_2)$, in a direction of $\vartheta_{1,2} = \cos^{-1}(\bar{\xi}_{1,2})$ with respect to the corresponding $x_{1,2}$-axis.

are GBs which are identified by their aperture planar field distributions over the $z = 0$ plane of the form [39], [42]

$$\widehat{B}_0(\mathbf{x}) = \exp\left[-jk\left(\bar{\boldsymbol{\xi}}^T\mathbf{x} + \frac{1}{2}\mathbf{x}^T\boldsymbol{\Gamma}_0\mathbf{x}\right)\right] \tag{2}$$

where $\bar{\boldsymbol{\xi}} = (\bar{\xi}_1, \bar{\xi}_2)$ are the expansion (directional) spectral variables and $\mathbf{x} = (x_1, x_2)$. Additional details regarding electromagnetic beam-type expansion and its spectral variables are given in Section V. Throughout this work, all vectors are column vectors and superscript T denotes the matrix (or the vector) transpose, so that the linear phase-term $\bar{\boldsymbol{\xi}}^T\mathbf{x} = \bar{\xi}_1 x_1 + \bar{\xi}_2 x_2$. In (2), $\boldsymbol{\Gamma}_0$ is a 2×2 complex symmetric matrix with a negative definite imaginary part. Here and henceforth, bold minuscule letters are used to denote vectors, whereas bold capital letters are used to denote matrices. Note that (2) consists of a Gaussian distribution with a linear phase term that causes the beam to tilt with respect to the initial $z = 0$ plane (see (27) as well as Fig. 2).

The paper layout is as follows. In the next section, we introduce a non-orthogonal coordinate system which is *a priori* matched to the field aperture distribution. In Section III, this coordinate system is utilized to obtain a novel (non-orthogonal) PWE whose localized solutions are obtained in Section IV (and termed tilted GBs). In Section V, we apply the scalar tilted GBs to beam-type expansion of *electromagnetic* waves. The reflection and transfer of these novel waveobjects through planar velocity discontinuity is discussed in Section VI. Finally, in Section VII a numerical example which demonstrates the enhanced accuracy of the tilted GBs over the conventional (orthogonal coordinate) ones, is given.

II. The Coordinate System

A. System Definition

We define a *non-orthogonal local coordinate system* as a system in which the transverse beam coordinates, x_{b_1} and x_{b_2}, lie on a plane parallel to the initial distribution plane at $z = 0$, whereas the longitudinal coordinate, z_b, is directed along the tilted beam-axis. We chose x_{b_1} and x_{b_2} to be orthogonal and moreover, parallel to x_1 and x_2 axes, respectively (see Fig. 1). Coordinates x_{b_1} and x_{b_2} form angles of ϑ_1 and ϑ_2 with the z_b coordinate, respectively. It is assumed that angles ϑ_1 and ϑ_2 remain constant for all observation points. In view of (2), they are related to the beam-expansion directional variables $\bar{\boldsymbol{\xi}}$ in (2) via

$$\bar{\boldsymbol{\xi}} = (\bar{\xi}_1, \bar{\xi}_2) = (\cos\vartheta_1, \cos\vartheta_2). \tag{3}$$

Denoting ϑ_3 as the angle between the z-axis and the paraxial propagation direction z_b, the unit-vector in the direction of z_b (in terms of the (x_1, x_2, z) coordinates) is given by

$$\hat{\mathbf{z}}_b = (\bar{\boldsymbol{\xi}}, \bar{\zeta}), \quad \bar{\zeta} = \cos\vartheta_3 = \sqrt{1 - \bar{\xi}_1^2 - \bar{\xi}_2^2} \tag{4}$$

where, here and henceforth, hat over a vector denotes a unit-vector. Using these definitions, the z_b-axis is identified as the *paraxial* propagation direction, and the transverse coordinates, x_{b_1} and x_{b_2}, lie on a plane parallel to the (x_1, x_2) plane and are centered at the intersection of the (x_{b_1}, x_{b_2}) plane with the z_b-axis. Therefore, the transformation from (x_1, x_2, z) to (x_{b_1}, x_{b_2}, z_b) is given by

$$x_{b_1} = x_1 - z\bar{\xi}_1/\bar{\zeta}, \quad x_{b_2} = x_2 - z\bar{\xi}_2/\bar{\zeta}, \quad z_b = z/\bar{\zeta} \tag{5}$$

and the observation vector $\mathbf{r}$ is given by

$$\mathbf{r} = x_{b_1}\hat{\mathbf{x}}_{b_1} + x_{b_2}\hat{\mathbf{x}}_{b_2} + z_b\hat{\mathbf{z}}_b \tag{6}$$

where $\hat{\mathbf{x}}_{b_1}$, $\hat{\mathbf{x}}_{b_2}$ and $\hat{\mathbf{z}}_b$ are the unit-vectors in the direction of the x_{b_1}, x_{b_2} and z_b axes, respectively, i.e., $\hat{\mathbf{x}}_{b_1} = \hat{\mathbf{x}}_1$, $\hat{\mathbf{x}}_{b_2} = \hat{\mathbf{x}}_2$, whereas $\hat{\mathbf{z}}_b$ is given in (4).

B. Metric Coefficients

The three so-called *unitary vectors* of the non-orthogonal system in (5), $\mathbf{a}_{1,2,3}$, are given by [44]

$$\mathbf{a}_1 = \frac{\partial\mathbf{r}}{\partial x_{b_1}} = \hat{\mathbf{x}}_{b_1}, \quad \mathbf{a}_2 = \frac{\partial\mathbf{r}}{\partial x_{b_2}} = \hat{\mathbf{x}}_{b_2}, \quad \mathbf{a}_3 = \frac{\partial\mathbf{r}}{\partial z_b} = \hat{\mathbf{z}}_b \tag{7}$$

and the g_{ij} elements of the 3×3 metric coefficients tensor $\mathbf{G}$ are given by $g_{ij} = \mathbf{a}_i \cdot \mathbf{a}_j$. By inserting (6) with (4) into (7),

we obtain the metric tensor of the non-orthogonal coordinate system

$$\mathbf{G} = [g_{ij}] = \begin{bmatrix} 1 & 0 & \bar{\xi}_1 \\ 0 & 1 & \bar{\xi}_2 \\ \bar{\xi}_1 & \bar{\xi}_2 & 1 \end{bmatrix} \tag{8}$$

its inverse

$$\mathbf{G^{-1}} = [g^{ij}] = \bar{\zeta}^{-2} \begin{bmatrix} 1-\bar{\xi}_2{}^2 & \bar{\xi}_1\bar{\xi}_2 & -\bar{\xi}_1 \\ \bar{\xi}_1\bar{\xi}_2 & 1-\bar{\xi}_1{}^2 & -\bar{\xi}_2 \\ -\bar{\xi}_1 & -\bar{\xi}_2 & 1 \end{bmatrix} \tag{9}$$

and its determinant

$$g = \det \mathbf{G} = \bar{\zeta}^2. \tag{10}$$

III. The Non-Orthogonal Domain Parabolic Equation

The Laplacian operator in a general non-orthogonal coordinate system (u^1, u^2, u^3) is given by [44]

$$\nabla^2 = \frac{1}{\sqrt{g}} \sum_{i=1}^{3} \sum_{j=1}^{3} \frac{\partial}{\partial u^i} \left[g^{ij}(u^1,u^2,u^3) \sqrt{g(u^1,u^2,u^3)} \frac{\partial}{\partial u^j} \right] \tag{11}$$

where g is given in (10) and g^{ij} are the (u^1, u^2, u^3) coordinate system metric coefficients in (9). By substituting (11) with (9) and (10) into (1), we obtain the Helmholtz equation in the non-orthogonal coordinates

$$\left(1-\bar{\xi}_2{}^2\right)\widehat{B}_{x_{b_1}x_{b_1}} + \left(1-\bar{\xi}_1{}^2\right)\widehat{B}_{x_{b_2}x_{b_2}} + 2\bar{\xi}_1\bar{\xi}_2\widehat{B}_{x_{b_1}x_{b_2}} - 2\bar{\xi}_1\widehat{B}_{x_{b_1}z_b} - 2\bar{\xi}_2\widehat{B}_{x_{b_2}z_b} + \widehat{B}_{z_bz_b} + k^2\bar{\zeta}^2\widehat{B} = 0, \tag{12}$$

where coordinate subscripts denote partial derivatives with respect to the coordinates, i.e., $\widehat{B}_{x_{b_1}} \equiv \partial\widehat{B}/\partial x_{b_1}$, $U_{x_{b_1}x_{b_2}} \equiv \partial^2 U/\partial x_{b_1}\partial x_{b_2}$, etc.

We are concerned with asymptotically evaluating the field $\widehat{B}(\mathbf{r})$ that satisfies the 3D Helmholtz equation (12) with boundary condition (2). High-frequency wave-fields propagate along predominant directions (ray trajectories). Thus, solutions of the Helmholtz equation at an arbitrary observation point $\mathbf{r}$ close to a ray trajectory, can be evaluated asymptotically by solving the PWE along the trajectory. By referring to boundary condition (2), we identify $\hat{\mathbf{z}}_b$ in (4) as the initial direction of the ray path which emanates from point $\mathbf{r} = (0,0,0)$ on the $z = 0$ plane. Therefore, we assume here that the wave field has the following *high-frequency* form

$$\widehat{B}(\mathbf{r}) = U(\mathbf{r}) \exp\left[-jks(\mathbf{r})\right] \tag{13}$$

where the Eikonal

$$s(\mathbf{r}) = z_b + \bar{\xi}_1 x_{b_1} + \bar{\xi}_2 x_{b_2} \tag{14}$$

is the projection of the observation vector $\mathbf{r}$ on the direction of the beam-axis z_b, and $U(\mathbf{r})$ denotes the ray-field amplitude. Using the ray-field (13), (14), we can evaluate the derivatives in (12)

$$\begin{aligned} \widehat{B}_{x_{b_1}} &= \left[U_{x_{b_1}} - j\bar{\xi}_1 kU\right] \exp\left[-jks(\mathbf{r})\right] \\ \widehat{B}_{x_{b_1}x_{b_1}} &= \left[U_{x_{b_1}x_{b_1}} - 2j\bar{\xi}_1 kU_{x_{b_1}} - \bar{\xi}_1{}^2 k^2 U\right] \\ &\quad \times \exp\left[-jks(\mathbf{r})\right] \end{aligned} \tag{15}$$

and so-forth for all partial derivatives in (12). Next, in the following derivation, following conventional paraxial ray-theory [3], [24], [25], we assume that the transverse coordinates, x_{b_1} and x_{b_2}, are on the order of $(1/\sqrt{k})$ (this assumption is justified by (27)). Under this assumption

$$\frac{\partial U(\mathbf{r})}{\partial x_{b_{1,2}}} \sim O(\sqrt{k}), \quad \frac{\partial^2 U(\mathbf{r})}{\partial x_{b_{1,2}}^2} \sim O(k). \tag{16}$$

By inserting (15) with (16) into (12), we find that the k^2 and $k^{3/2}$ order elements cancel out, so that the parabolic equation is obtained by setting the next higher order, the k-coefficient, to zero. This procedure yields

$$\left(1-\bar{\xi}_2^2\right)U_{x_{b_1}x_{b_1}} + 2\bar{\xi}_1\bar{\xi}_2 U_{x_{b_1}x_{b_2}} + \left(1-\bar{\xi}_1^2\right)U_{x_{b_2}x_{b_2}} - 2jk\bar{\zeta}^2 U_{z_b} = 0. \tag{17}$$

Equation (17) is termed the *Non-orthogonal Domain parabolic equation* (NoDope). Note, that by setting $\vartheta_1 = \vartheta_2 = \pi/2$ (namely $\bar{\xi}_1 = \bar{\xi}_2 = 0$) in (17), the latter reduces to the well-known PWE in orthogonal coordinates [3], [24], [25].

IV. Tilted Gaussian Beams

A. Field Solutions

In view of the initial field distribution in (2), we are seeking localized beam solutions of the NoDope which carry Gaussian decay away from their $\hat{\mathbf{z}}_b$ axes. Therefore, we assume a beam-type field of the form

$$U(\mathbf{r}) = A(z_b) \exp\left[-jk\frac{1}{2}\mathbf{x}_b^T\mathbf{\Gamma}(z_b)\mathbf{x}_b\right] \tag{18}$$

where $\mathbf{x}_b = (x_{b_1}, x_{b_2})$ and the so-called complex curvature matrix $\mathbf{\Gamma}$ is a complex symmetrical matrix with Γ_{ij} denoting its (i,j)th element so that the exponent in (18) is of the quadratic form $\mathbf{x}_b^T\mathbf{\Gamma}\mathbf{x}_b = x_{b_1}^2\Gamma_{11} + 2x_{b_1}x_{b_2}\Gamma_{12} + x_{b_2}^2\Gamma_{22}$. The matrix $\mathbf{\Gamma}$ has a negative definite imaginary part, hence beam-field (18) exhibits a Gaussian decay over a plane that is tilted by $\bar{\boldsymbol{\xi}} = (\cos\vartheta_1, \cos\vartheta_2)$ with respect to the beam-axis direction $\hat{\mathbf{z}}_b$. Beam-fields of form (18) (with (13)) which carry initial Gaussian distributions over the tilted $z = 0$ plane are termed here *tilted GBs*. Using beam-field (18), we may now evaluate

$$\begin{aligned} U_{x_{b_1}x_{b_1}} &= \left[-jk\Gamma_{11} - k^2\left(x_{b_1}\Gamma_{11} + x_{b_2}\Gamma_{12}\right)^2\right]U \\ U_{x_{b_2}x_{b_2}} &= \left[-jk\Gamma_{22} - k^2\left(x_{b_1}\Gamma_{12} + x_{b_2}\Gamma_{22}\right)^2\right]U \\ U_{x_{b_1}x_{b_2}} &= \left[-jk\Gamma_{12} - k^2\left(x_{b_1}^2\Gamma_{11}\Gamma_{12} + x_{b_1}x_{b_2}\left(\Gamma_{11}\Gamma_{22} + \Gamma_{12}^2\right) + x_{b_2}^2\Gamma_{12}\Gamma_{22}\right)\right]U \\ U_{z_b} &= \left[-jk\mathbf{x}_b^T\mathbf{\Gamma}'(z_b)\mathbf{x}_b/2 + A'(z_b)/A(z_b)\right]U \end{aligned} \tag{19}$$

where the prime denotes a derivative with respect to the argument. Next, we insert all U partial derivatives in (19) into NoDope (17) and collect elements of the same order in x_{b_1} and x_{b_2}, which results in

$$\begin{aligned}&\Big[\left(1-\bar{\xi}_2^2\right)\Gamma_{11}^2+2\bar{\xi}_1\bar{\xi}_2\Gamma_{11}\Gamma_{12}\\&\quad+\left(1-\bar{\xi}_1^2\right)\Gamma_{12}^2+\bar{\zeta}^2\Gamma'_{11}(z_b)\Big]x_{b_1}^2\\&\quad+\Big[\left(1-\bar{\xi}_1^2\right)\Gamma_{22}^2+2\bar{\xi}_1\bar{\xi}_2\Gamma_{12}\Gamma_{22}\\&\qquad+\left(1-\bar{\xi}_2^2\right)\Gamma_{12}^2+\bar{\zeta}^2\Gamma'_{22}(z_b)\Big]x_{b_2}^2\\&\quad+\Big[2\left(1-\bar{\xi}_2^2\right)\Gamma_{11}\Gamma_{12}+2\left(1-\bar{\xi}_1^2\right)\Gamma_{12}\Gamma_{22}\\&\qquad+2\bar{\xi}_1\bar{\xi}_2\left(\Gamma_{11}\Gamma_{22}+\Gamma_{12}^2\right)+2\bar{\zeta}^2\Gamma'_{12}(z_b)\Big]x_{b_1}x_{b_2}\\&\quad+\Big[\Big(\mathrm{trace}\{\boldsymbol{\Gamma}\}-\bar{\xi}_2^2\Gamma_{11}+2\bar{\xi}_1\bar{\xi}_2\Gamma_{12}-\bar{\xi}_1^2\Gamma_{22}\Big)\\&\qquad+2\bar{\zeta}^2A'(z_b)/A(z_b)\Big](jk)^{-1}=0.\end{aligned}\tag{20}$$

Relation (20) holds for all $\mathbf{x}_b$ near the beam-axis, and therefore, consists of four equations which are obtained by setting all four coefficients to zero. These equations may be written in a compact way by defining

$$\boldsymbol{\Upsilon}=\begin{bmatrix}\left(1-\bar{\xi}_2^2\right)&\bar{\xi}_1\bar{\xi}_2\\\bar{\xi}_1\bar{\xi}_2&\left(1-\bar{\xi}_1^2\right)\end{bmatrix}.\tag{21}$$

The first three equations yield a vector Riccati-type equation for $\boldsymbol{\Gamma}$

$$\boldsymbol{\Gamma}\boldsymbol{\Upsilon}\boldsymbol{\Gamma}+\bar{\zeta}^2\boldsymbol{\Gamma}'(z_b)=0\tag{22}$$

whereas setting the last (free) term in (20) to zero yields

$$\mathrm{trace}(\boldsymbol{\Upsilon}\boldsymbol{\Gamma})A(z_b)+2\bar{\zeta}^2A'(z_b)=0.\tag{23}$$

Equation (23) serves as the amplitude $A(z_b)$ equation once the Ricatti equation (22) is solved for $\boldsymbol{\Gamma}$. The procedure of solving the Ricatti equation is straightforward in that by setting $\boldsymbol{\Gamma}(z_b)=\mathbf{Q}^{-1}(z_b)$, relation (22) transforms into $\mathbf{Q}'-\bar{\zeta}^{-2}\boldsymbol{\Upsilon}=0$. Thus

$$\boldsymbol{\Gamma}(z_b)=\mathbf{Q}^{-1}(z_b)=\left[\boldsymbol{\Gamma}_0^{-1}+\bar{\zeta}^{-2}\boldsymbol{\Upsilon}z_b\right]^{-1}\tag{24}$$

where $\boldsymbol{\Gamma}_0$ is the complex curvature matrix of the initial field distribution over the $z_b=0$ plane in (2). The beam amplitude, $A(z_b)$, may now be found by inserting $\mathrm{trace}[\mathbf{Q}'\mathbf{Q}^{-1}]=\ln'[\det(\mathbf{Q})]$, as well as (24), into (23), which results in the linear ODE

$$A(z_b)\ln'[\det(\mathbf{Q})]+2A'(z_b)=0.\tag{25}$$

Using a straightforward separation of variables, we obtain

$$A(z_b)=\sqrt{\frac{\det[\boldsymbol{\Gamma}(z_b)]}{\det[\boldsymbol{\Gamma}_0]}}.\tag{26}$$

The tilted GB field may now be written explicitly by using (24) and (26) in (18), and inserting into (13), which yields

$$\begin{aligned}\widehat{B}(\mathbf{r})&=\sqrt{\frac{\det[\boldsymbol{\Gamma}(z_b)]}{\det[\boldsymbol{\Gamma}_0]}}\exp\left[-jk\Psi(\mathbf{r}_b)\right]\\\Psi(\mathbf{r}_b)&=s+\frac{1}{2}\mathbf{x}_b^T\boldsymbol{\Gamma}(z_b)\mathbf{x}_b\end{aligned}\tag{27}$$

where s is given in (14), $\mathbf{x}_b=(x_{b_1},x_{b_2})$ and $\boldsymbol{\Gamma}(z_b)$ is given in (24). By setting $z_b=0$, we verify that GB (27) satisfies the aperture field distribution in (2) exactly. This type of GB waveobjects exhibits frequency-independent collimation (Rayleigh) distance and therefore have been termed *iso-diffracting* [45] (see also (34)). The iso-diffracting feature makes these waveobjects highly suitable for UWB radiation representations [31], [33], [34], [39]–[41], [46].

B. Field Parametrization

Applying radially-symmetric Gaussian windows to some aperture field distribution results in a beam-type expansion in which the propagating waveobjects are *iso-axial* tilted GBs. Such GBs are characterized by a diagonal initial complex curvature matrix of the form [39], [42], [43]

$$\boldsymbol{\Gamma}_0=\mathbf{I}\Gamma_0,\quad \Gamma_0=(-Z+jF)^{-1},\quad F>0\tag{28}$$

where $\mathbf{I}$ denotes the 2×2 unity matrix. The complex curvature matrix is obtained by using (28) in (24), which yields (29) at bottom of page. The real and imaginary parts of the complex iso-axial curvature matrix may be diagonalized simultaneously by rotating the $\mathbf{x}_b$-axes over constant z_b-planes, by a *z_b-independent* angle Φ_c, where

$$\tan 2\Phi_c=2\bar{\xi}_1\bar{\xi}_2/\left(\bar{\xi}_1^2-\bar{\xi}_2^2\right)\tag{30}$$

i.e., $\cos\Phi_c=\bar{\xi}_1/\bar{\xi}$ and $\sin\Phi_c=\bar{\xi}_2/\bar{\xi}$ with $\bar{\xi}=\sqrt{\bar{\xi}_1{}^2+\bar{\xi}_2{}^2}$. Angle Φ_c is identified as the angle between the x_1-axis and the projection of the z_b-axis on the (x_1,x_2) plane. The resulting rotation transformation of $\mathbf{x}_b$ to the transverse coordinates $\mathbf{x}_c=(x_{c_1},x_{c_2})$ in which $\boldsymbol{\Gamma}$ is a diagonal matrix is given by

$$\mathbf{x}_c=\mathbf{T}\mathbf{x}_b,\quad \mathbf{T}=\begin{bmatrix}\cos\Phi_c&\sin\Phi_c\\-\sin\Phi_c&\cos\Phi_c\end{bmatrix}.\tag{31}$$

$$\boldsymbol{\Gamma}(z_b)=\begin{bmatrix}-Z+jF+\left(1-\bar{\xi}_2^2\right)\bar{\zeta}^{-2}z_b&\bar{\xi}_1\bar{\xi}_2\bar{\zeta}^{-2}z_b\\\bar{\xi}_1\bar{\xi}_2\bar{\zeta}^{-2}z_b&-Z+jF+\left(1-\bar{\xi}_1^2\right)\bar{\zeta}^{-2}z_b\end{bmatrix}^{-1}.\tag{29}$$

Thus, the quadratic phase in (27) in the $\mathbf{x}_c$ coordinates, is given by

$$\mathbf{x}_b^T\mathbf{\Gamma}\mathbf{x}_b = \mathbf{x}_c^T\mathbf{\Gamma}_c\mathbf{x}_c, \quad \mathbf{\Gamma}_c = \mathbf{T}\mathbf{\Gamma}\mathbf{T}^{-1} \tag{32}$$

and, by using (29) with (31) in (32), we obtain

$$\mathbf{\Gamma}_c(z_b) = \begin{bmatrix} (z_b\bar{\zeta}^{-2} - Z + jF)^{-1} & 0 \\ 0 & (z_b - Z + jF)^{-1} \end{bmatrix} \tag{33}$$

where Z and F are given in (28).

Using (33) with (32) in (27), we find that the iso-axial tilted GB exhibits (pure) quadratic decay in the (x_{c_1}, x_{c_2}) directions with corresponding e^{-1} beam-widths of

$$W_{1,2}(z_b) = D_{1,2}\sqrt{1 + \frac{(z_b - Z_{1,2})^2}{F_{1,2}^2}} \tag{34}$$

where

$$Z_1 = Z\bar{\zeta}^2, \quad Z_2 = Z, \qquad F_1 = F\bar{\zeta}^2, \quad F_2 = F \tag{35}$$

and $D_{1,2} = \sqrt{8F_{1,2}/k}$ are the principal beam-widths at the waists. By using (34), we identify $F_{1,2}$ and $Z_{1,2}$ as the beam *collimation-lengths* and *waist-locations* on the $(z_b, x_{c_{1,2}})$ principal planes, respectively. On the $(z_b, x_{c_{1,2}})$ planes, the beam field remains collimated near the waists where $|z_b - Z_{1,2}| \ll F_{1,2}$, whereas away from the waists, it opens up along constant diffraction angles of $\Theta_{1,2} = (kF_{1,2}/8)^{-1/2}$ in $x_{c_{1,2}}$ axes.

V. Applications to Electromagnetic Waves

Expansion of electromagnetic (EM) fields using GBs has been applied in [47]–[49] for analyzing large reflector antennas in which the expansion coefficients were obtained by numerically matching GBs to the far zone field of the feed antenna. However these methods do not employ *exact* field expansion schemes and therefore, cannot be applied for near-field analysis, or in exact field calculations. Exact EM field beam-type expansion was investigated in [43], but the asymptotic EM beam propagators presented there were limited to validity of the conventional (orthogonal coordinates) paraxial approximation, i.e., for small ϑ_3 angles. Here, we briefly describe the EM expansion scheme presented in [43] and then derive *accurate* asymptotics in term of scalar *tilted GBs* in (27).

The discrete exact expansion scheme synthesizes the time-harmonic EM field propagating in $z \geq 0$ due to sources in $z < 0$, given the transverse electric field over $z = 0$ plane

$$\mathbf{E}_0(\mathbf{x}) = E_1(\mathbf{x})\hat{\mathbf{x}}_1 + E_2(\mathbf{x})\hat{\mathbf{x}}_2. \tag{36}$$

The propagation medium is homogeneous with ϵ_0 and μ_0 denoting the free space permittivity and permeability, respectively. The expansion scheme is constructed on a discrete spatial-directional lattice $\bar{\mathbf{x}} = (\bar{x}_1, \bar{x}_2)$ and $\bar{\boldsymbol{\xi}} = (\bar{\xi}_1, \bar{\xi}_2)$, where

$$(\bar{\mathbf{x}}, \bar{\boldsymbol{\xi}}) = (m_1\Delta\bar{x}_1, m_2\Delta\bar{x}_2, n_1\Delta\bar{\xi}_1, n_2\Delta\bar{\xi}_2) \tag{37}$$

with $(\Delta\bar{x}_1, \Delta\bar{x}_2)$ and $(\Delta\bar{\xi}_1, \Delta\bar{\xi}_2)$ denoting the unit-cell dimensions in the (x_1, x_2) and (ξ_1, ξ_2) coordinates, respectively. The index $\boldsymbol{\mu} = (m_1, m_2, n_1, n_2)$ is used to tag the lattice points (see Fig. 2). These unit-cell dimensions satisfy

$$k\Delta\bar{x}_1\Delta\bar{\xi}_1 = 2\pi\nu_1, \quad k\Delta\bar{x}_2\Delta\bar{\xi}_2 = 2\pi\nu_2 \tag{38}$$

where $0 \leq \nu_{1,2} \leq 1$ are the overcompleteness parameters in the $x_{1,2}$ axes.

The initial field distribution is expanded using a spatially-localized *synthesis window*, $\psi(\mathbf{x})$, whereas the expansion coefficients are obtained by evaluating the inner product of the initial distribution with the corresponding *analysis window* $\varphi(\mathbf{x})$. Several methods for evaluating the analysis window from the synthesis window are provided in [39]. Following [43], the coefficients vector of the initial electric field is given by

$$\mathbf{a}^{\boldsymbol{\mu}} = a_1^{\boldsymbol{\mu}}\hat{\mathbf{x}}_1 + a_2^{\boldsymbol{\mu}}\hat{\mathbf{x}}_2 = \int d^2x\mathbf{E}_0(\mathbf{x})\varphi^*(\mathbf{x};\boldsymbol{\mu}) \tag{39}$$

where the function set $\varphi(\mathbf{x};\boldsymbol{\mu})$ is related to the analysis window $\varphi(\mathbf{x})$ via

$$\varphi(\mathbf{x};\boldsymbol{\mu}) = \varphi(\mathbf{x} - \bar{\mathbf{x}})\exp\left[-jk\bar{\boldsymbol{\xi}}^T(\mathbf{x} - \bar{\mathbf{x}})\right]. \tag{40}$$

Using the coefficient vector in (39), the electric field expansion is given by

$$\mathbf{E}(\mathbf{r}) = \sum_{\boldsymbol{\mu}} a_1^{\boldsymbol{\mu}}\mathbf{E}_1^B(\mathbf{r};\boldsymbol{\mu}) + a_2^{\boldsymbol{\mu}}\mathbf{E}_2^B(\mathbf{r};\boldsymbol{\mu}) \tag{41}$$

where the electric fields of the *EM beam propagators*, $\mathbf{E}_1^B(\mathbf{r};\boldsymbol{\mu})$ and $\mathbf{E}_2^B(\mathbf{r};\boldsymbol{\mu})$, are obtained from the *scalar* beam propagator $B(\mathbf{r};\boldsymbol{\mu})$ via

$$\begin{aligned} \mathbf{E}_1^B(\mathbf{r};\boldsymbol{\mu}) &= \left(\hat{\mathbf{x}}_1 - \hat{\mathbf{z}}\partial_{x_1}\partial_z^{-1}\right)B(\mathbf{r};\boldsymbol{\mu}) \\ \mathbf{E}_2^B(\mathbf{r};\boldsymbol{\mu}) &= \left(\hat{\mathbf{x}}_2 - \hat{\mathbf{z}}\partial_{x_2}\partial_z^{-1}\right)B(\mathbf{r};\boldsymbol{\mu}). \end{aligned} \tag{42}$$

Here we denote, $\partial_{x_1} = \partial/\partial x_1$, $\partial_z^{-1} = \int^z dz'$, etc. Note that these operators may be evaluated asymptotically in closed form for Gaussian windows (see (48) and (49)). The scalar beam propagator, $B(\mathbf{r};\boldsymbol{\mu})$, satisfies the Helmholtz equation (1) subject to the aperture distribution over the $z = 0$ plane

$$\widehat{B}_0(\mathbf{x};\boldsymbol{\mu}) = \psi(\mathbf{x} - \bar{\mathbf{x}})\exp\left[-jk\bar{\boldsymbol{\xi}}^T(\mathbf{x} - \bar{\mathbf{x}})\right] \tag{43}$$

where $\psi(\mathbf{x})$ is the synthesis window. Equation (41) together with (42) represent the electric field, $\mathbf{E}(\mathbf{r})$, as a discrete superposition of EM beam waveobjects, $\mathbf{E}_1^B$ and $\mathbf{E}_2^B$, which are the electric field propagators due to the initial electric field x_1 and x_2 components present over the $z = 0$ plane, respectively.

The corresponding magnetic field in $z \geq 0$ is is obtained by inserting (41) with (42) into Faraday's law, $\mathbf{H} = (-j\omega\mu_0)^{-1}\nabla \times \mathbf{E}$. This yields

$$\mathbf{H}(\mathbf{r}) = \sum_{\boldsymbol{\mu}} a_1^{\boldsymbol{\mu}}\mathbf{H}_1^B(\mathbf{r};\boldsymbol{\mu}) + a_2^{\boldsymbol{\mu}}\mathbf{H}_2^B(\mathbf{r};\boldsymbol{\mu}) \tag{44}$$

where the expansion coefficients are given in (39) and the magnetic field of the *EM beam propagators*, $\mathbf{H}_1^B$ and $\mathbf{H}_2^B$, are given by

$$\mathbf{H}_1^B(\mathbf{r};\boldsymbol{\mu}) = \frac{-j}{k\eta_0}\left[\hat{\mathbf{x}}_1\partial^2_{x_1x_2}\partial_z^{-1} - \hat{\mathbf{x}}_2\left(\partial^2_{x_1}\partial_z^{-1}+\partial_z\right)+\hat{\mathbf{z}}\partial_{x_2}\right] \times B(\mathbf{r};\boldsymbol{\mu})$$
$$\mathbf{H}_2^B(\mathbf{r};\boldsymbol{\mu}) = \frac{-j}{k\eta_0}\left[\hat{\mathbf{x}}_1\left(\partial^2_{x_2}\partial_z^{-1}+\partial_z\right) - \hat{\mathbf{x}}_2\partial^2_{x_1x_2}\partial_z^{-1} - \hat{\mathbf{z}}\partial_{x_1}\right] \times B(\mathbf{r};\boldsymbol{\mu}) \quad (45)$$

and where $\eta_0 = \sqrt{\mu_0/\epsilon_0} = 120\pi\Omega$ is the free space wave impedance.

Next, the general spectral representation in (41) is applied for the special case of Gaussian windows. By choosing a Gaussian synthesis window

$$\psi(\mathbf{x}) = \exp\left(-jk\frac{1}{2}\mathbf{x}^T\boldsymbol{\Gamma}_0\mathbf{x}\right) \quad (46)$$

and inserting it into (43), we find that the scalar beam propagators, $B(\mathbf{r};\boldsymbol{\mu})$, satisfy the Helmholtz equation subject to the initial distribution (2). Hence, these waveobjects are recognized as the *tilted GBs* in (27) subject to a transverse shift by $\bar{\mathbf{x}}$ to the spectral lattice (i.e., by replacing $\mathbf{x}$ with $(\mathbf{x}-\bar{\mathbf{x}})$ in (5)).

The *asymptotic* paraxial tilted GB can be used for evaluating the *EM* Gaussian propagators by inserting (27) into (42), and evaluating the partial derivatives in closed form. Thus, by using (5) and maintaining only terms of the highest asymptotic order, we may replace

$$\partial_{x_1} \sim -jk\bar{\xi}_1, \quad \partial_z \sim -jk\bar{\zeta}, \quad \partial_z^{-1} \sim (-jk\bar{\zeta})^{-1} \quad (47)$$

such that the resulting asymptotic electric field propagators are given by

$$\mathbf{E}^B_{1,2}(\mathbf{r};\boldsymbol{\mu}) \sim \frac{1}{\bar{\zeta}}[\hat{\mathbf{x}}_{1,2}\bar{\zeta} - \hat{\mathbf{z}}\bar{\xi}_{1,2}]B(\mathbf{r};\boldsymbol{\mu}) \quad (48)$$

In a similar manner, the magnetic field, $\mathbf{H}_1^B(\mathbf{r})$, is obtained by using (47) in (45), giving

$$\mathbf{H}_1^B(\mathbf{r};\boldsymbol{\mu}) \sim \frac{-1}{\eta_0\bar{\zeta}}\left[\hat{\mathbf{x}}_1\bar{\xi}_1\bar{\xi}_2+\hat{\mathbf{x}}_2\left(\bar{\xi}_2^2-1\right)+\hat{\mathbf{z}}\bar{\xi}_2\bar{\zeta}\right]B(\mathbf{r};\boldsymbol{\mu})$$
$$\mathbf{H}_2^B(\mathbf{r};\boldsymbol{\mu}) \sim \frac{1}{\eta_0\bar{\zeta}}\left[\hat{\mathbf{x}}_1\left(\bar{\xi}_1^2-1\right)+\hat{\mathbf{x}}_2\bar{\xi}_1\bar{\xi}_2+\hat{\mathbf{z}}\bar{\xi}_1\bar{\zeta}\right]B(\mathbf{r};\boldsymbol{\mu}). \quad (49)$$

VI. Reflection and Transmission From Planar Discontinuities

In this section, we explore a 2D tilted GB incidence on planar wave-speed discontinuity as well as the resulting reflected and transmitted fields. The incident scalar field propagating in v_1 medium is assumed to have the 2D tilted beam canonical form, which is obtained by setting $\Gamma_0^{12} = \Gamma_0^{21} = \Gamma_0^{22} = 0$ in GB (27). The scalar field satisfies continuity of the total field at the interface, as well as of $\chi_{1,2}^{-1}\partial/\partial n$. These boundary conditions correspond to an *electromagnetic* field incidence where $\chi_{1,2}$ correspond to either $\epsilon_{1,2}$ or $\mu_{1,2}$ for a TE or TM field incidence, respectively, and the scalar field being either the electric (TE) or magnetic (TM) field component in the direction normal to the plane of incidence, $\hat{\mathbf{x}}_2$. Subscripts 1,2 denote quantities on either side of the interface (see Fig. 3).

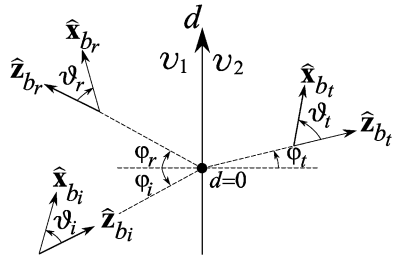

Fig. 3. Scattering of the tilted GB from a planar discontinuity in the medium's velocity profile. The reflected and transmitted fields are tilted GBs which are characterized by the corresponding φ (beam-axis direction) and ϑ (non-orthogonal system tilt) parameters. d is a length coordinate along the interface.

We assume that both reflected and transmitted fields are all of the same canonical form and differ only by amplitude A, Eikonal s and initial complex curvature Γ_0. Therefore, we may write

$$\widehat{B}_\alpha(\mathbf{r}) = A_\alpha(z_{b_\alpha})\exp\left[-jk_\alpha\Psi_\alpha(\mathbf{r}_{b_\alpha})\right]$$
$$\Psi_\alpha(\mathbf{r}_b) = s_\alpha + \frac{1}{2}\Gamma_\alpha(z_{b_\alpha})x^2_{b_\alpha} \quad (50)$$

where subscript $\alpha = i, r$, and t denote *incident*, *reflected* and *transmitted* wave constituents, respectively. Note that $v_i = v_r = v_1$ whereas $v_t = v_2$ where v_1 and v_2 are the wave velocities on either side of the interface. Each tilted GB is identified by ϑ_α which denotes the angle between z_{b_α} and x_{b_α} in the non-orthogonal coordinate systems, and φ_α which denotes the incidence, reflection or transmission conventional (snell) angles. In order to compare the beam-fields along the interface, we express them as a function of the length coordinate along this interface, which is denoted by d. Without loss of generality, we assume that $z_{b_\alpha} = 0$ and $d = 0$ at the incident point, i.e., at the intersection of the incident beam-axis and the scattering interface. Using the 2D analog of the tilted beam complex curvature in (24), we may write

$$\Gamma_\alpha(z_{b_\alpha}) = \left[\Gamma_\alpha^{-1}(0) + \csc^2\vartheta_\alpha z_{b_\alpha}\right]^{-1} \quad (51)$$

where $\Gamma_\alpha(0)$ denotes the tilted beam-field complex curvature at the incident point, $d = 0$. Using simple trigonometry, we may express the beam-field coordinates along the interface in terms of d as

$$x_{b_\alpha} = \frac{\cos\varphi_\alpha}{\sin\vartheta_\alpha}d, \quad z_{b_\alpha} = -\frac{\cos(\varphi_\alpha+\vartheta_\alpha)}{\sin\vartheta_\alpha}d. \quad (52)$$

By applying a continuity condition to the total field, it can be concluded that the three phases of $\widehat{B}_\alpha$ should all coincide at the interface. By using (52) in (50) and comparing the *linear* phase-term, we obtain the conventional *Snell's* law

$$\varphi_i = \varphi_r, \quad v_2\sin\varphi_i = v_1\sin\varphi_t \quad (53)$$

while the *quadratic* phase-term in (51) yields

$$\frac{\cos(\varphi_t+\vartheta_t)}{\sin\vartheta_t} = \frac{v_1}{v_2}\frac{\cos^2\varphi_t}{\cos^2\varphi_i}\frac{\cos(\varphi_i+\vartheta_i)}{\sin\vartheta_i}. \quad (54)$$

The transmitted complex curvature is given by

$$\Gamma_t(0) = \Gamma_i(0)\frac{\cos^2\varphi_i}{\sin^2\vartheta_i}\frac{\sin^2\vartheta_t}{\cos^2\varphi_t}. \tag{55}$$

Note that relation (54) may be further simplified in the form

$$\sin\vartheta_t = \frac{\cos\varphi_t}{\sqrt{\cos^2\varphi_t + (C+\sin\varphi_t)^2}} \tag{56}$$

where

$$C = \frac{v_1}{v_2}\frac{\cos^2\varphi_t}{\cos^2\varphi_i}\frac{\cos(\varphi_i+\vartheta_i)}{\sin\vartheta_i}. \tag{57}$$

One may readily observe that the righthand side of (56) is smaller than one. Hence, a real solution for ϑ_t is assured for incident angles smaller than the critical angle, where φ_t is real. Once ϑ_t is found from either (54) or (56), the transmitted complex curvature, $\Gamma_t(0)$, is obtained from (55). Following essentially the same procedure, we obtain for the reflected field

$$\vartheta_r = \vartheta_i \quad \Gamma_r(0) = \Gamma_i(0). \tag{58}$$

Finally, we apply the continuity condition to the total field over the interface, as well as to its weighted normal derivative, $\chi_{1,2}^{-1}\partial/\partial n$, and obtain the well-known reflection and transmission amplitude coefficient relations

$$A_r = A_i R, \qquad A_t = A_i T \tag{59}$$

where R and T are the conventional fresnel reflection and transmission coefficients

$$R = \frac{\chi_1 v_1\cos\varphi_i - \chi_2 v_2\cos\varphi_t}{\chi_1 v_1\cos\varphi_i + \chi_2 v_2\cos\varphi_t}, \qquad T = 1+R. \tag{60}$$

Note that for the TE case $\chi v = \sqrt{\mu/\epsilon} = \eta$, whereas, the TM component yields $\chi v = \sqrt{\epsilon/\mu} = \eta^{-1}$.

VII. Numerical Example

The general formulation in Section IV is demonstrated in this section by a numerical simulation of a 2D tilted GB which is obtained by setting $\Gamma_0^{12} = \Gamma_0^{21} = \Gamma_0^{22} = 0$ in (27). Hence, the matrix $\mathbf{\Gamma}_0$ is transformed into the scalar Γ_0, the vectors $\mathbf{x}$, $\mathbf{x}_b$, and $\bar{\boldsymbol{\xi}}$, are replaced by the scalars x, x_b, and $\bar{\xi}$, respectively, and the initial tilt angles $\vartheta_{1,2}$ by ϑ. The initial field distribution is given by (2), with

$$\Gamma_0 = (-Z+jF)^{-1}. \tag{61}$$

The simulation compares the error of the tilted GB to the error of the conventional (orthogonal coordinate) GB solution, all with respect to a reference solution according to the following details.

A. Tilted GB Simulation

The 2D complex curvature, $\Gamma(z_b)$, is obtained by using (61) in (24), giving

$$\Gamma(z_b) = (z_b\bar{\zeta}^{-2} - Z + jF)^{-1} \tag{62}$$

where $\bar{\zeta} = \sqrt{1-\bar{\xi}^2}$. By inserting (62) into the 2D analogue of (27), we obtain the 2D asymptotically-exact tilted GB

$$\widehat{B}_{tilted} = \sqrt{\frac{1}{1+\Gamma_0 z_b/\bar{\zeta}^2}}\exp\left\{-jk\left[s+\frac{1}{2}\Gamma(z_b)x_b^2\right]\right\}. \tag{63}$$

For a given observation point, $\mathbf{r} = (x,z)$, the local non-orthogonal coordinates are given by $x_b = n/\bar{\zeta}$ and $z_b = s - n\bar{\xi}/\bar{\zeta}$ where n is a coordinate normal to the beam-axis and s is the distance between the exit point to the intersection point of the normal coordinate and the beam-axis. Thus, the local orthogonal coordinates are given by

$$s = \bar{\xi}x + \bar{\zeta}z \quad n = \bar{\zeta}x - \bar{\xi}z. \tag{64}$$

B. Conventional GB Simulation

We compare the tilted GB (63) to the conventional one which is obtained by projecting the initial complex curvature Γ_0 over a plane perpendicular to the beam axis direction $\hat{\mathbf{z}}_b$ [3], [26]. Hence, the projected complex curvature matrix is given by $\Gamma_{n_0} = \Gamma_0/\bar{\zeta}^2$ and the conventional (orthogonal coordinates) GB, $\widehat{B}_{conv}$ is given by

$$\widehat{B}_{orth} = \sqrt{\frac{1}{1+\Gamma_{n_0}s}}\exp\left\{-jk\left[s+\frac{1}{2}\Gamma_n(s)n^2\right]\right\}$$
$$\Gamma_n(s) = \frac{\Gamma_{n_0}}{1+\Gamma_{n_0}s} \tag{65}$$

where s and n are given in (64).

C. Reference Field Solution

The reference field solution is obtained by evaluating numerically the plane-wave spectrum integral corresponding to the aperture distribution (2), i.e.,

$$\widehat{B}_{ref}(x,z) = \sqrt{\frac{-jk}{2\pi\Gamma_0}}\int d\xi\exp\left[-jkq(\xi)\right]$$
$$q(\xi) = -\frac{(\bar{\xi}-\xi)^2}{2\Gamma_0} + \zeta z + \xi x \tag{66}$$

with $\zeta(\xi) = \sqrt{1-\xi^2}$, $\mathrm{Im}\zeta \geq 0$, and Γ_0 is given in (61). The $(-\infty,\infty)$ integration in (66) is replaced with a truncated integration over an effective contribution interval around the phase on-axis stationary point, $\xi_s = \bar{\xi}$, i.e., $[\bar{\xi}-\Delta\xi, \bar{\xi}+\Delta\xi]$ with $\Delta\xi = \sqrt{M/k\mathrm{Im}(\Gamma_0^{-1})} = \sqrt{M/Fk}$ where e^{-M} is the required threshold for spectrum attenuation. The sampling rate, $\delta\xi$, is chosen according to the condition $\delta\xi \ll \Delta\xi/M$ (which is valid in the collimation zone), implying that the integrand oscillation period is much larger than the sampling rate and that the integrand attenuation in the sampled interval is sufficient for convergence. It was found that in order to an achieve accuracy range of 10^{-5}, it is sufficient to chose $M = 5$ and $\delta\xi = 10^{-3}\Delta\xi/M$.

D. Error Comparison

In order to verify the accuracy of the tilted GB solution, we compare the $\mathbb{L}_2$ error norm of the tilted GB in (63) with respect to the reference field in (66), to the corresponding $\mathbb{L}_2$ error norm

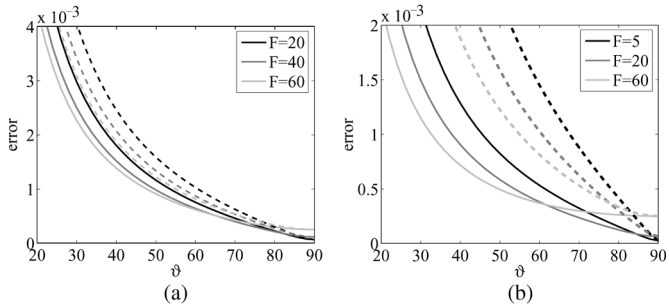

Fig. 4. $\mathbb{L}_2$ error with respect to the reference solution as a function of ϑ. Continuous and dashed lines are corresponding to the tilted GB in (63) and the conventional GB in (65), respectively. (a) $s_m/F_b = 1/2$; (b) $s_m/F_b = 1/4$.

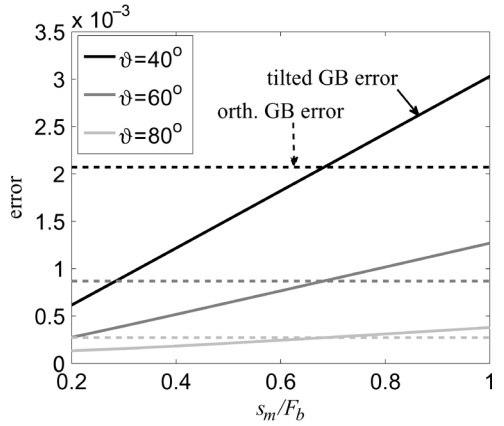

Fig. 5. $\mathbb{L}_2$ error with respect to the reference solution as a function of the on-axis location, s_n/F_b, for different ϑ values. Continuous and dashed lines correspond to the tilted GB (63) and conventional GB (65) errors, respectively. The results clearly show that the tilted GBs exhibit enhanced accuracy over the conventional ones in the well-collimated zone.

of the conventional GB solution in (65). The $\mathbb{L}_2$ error norm between GB B and the reference GB, B_{ref}, is evaluated along line L according to

$$\mathbb{L}_2[B, B_{ref}] = \sqrt{\frac{1}{L}\int_L |B(l) - B_{ref}(l)|^2 \, dl} \qquad (67)$$

where B stands for B_{orth} in (65) or B_{tilted} in (63).

In Fig. 4, the $\mathbb{L}_2$ error norm is evaluated along an observation line which is *normal* to the beam-axis and located at an on-axis distance of s_m from the initial $z = 0$ plane. The figure plots the error as a function of the beam-axis angle ϑ for different initial complex curvatures Γ_0, all with $\mathrm{Re}\Gamma_0 = 0$, setting the GB waists location to $z = 0$. The curves are arranged in couples with the continuous and dashed lines corresponding to the tilted GB error and the conventional one, respectively. Each of the curve couples in Fig. 4 share a gray shade which correspond to different beam parameter $F = -\mathrm{Im}(\Gamma_0^{-1})$ (recall from (35) that the collimation-length $F_b = F\bar{\zeta}^2 = F\sin^2\vartheta$). The observation line is located at 1/2 or 1/4 of the corresponding collimation-length in Figs. 4(a) and 4(b), respectively. The plots are evaluated for $k = 1e3[1/m]$. These figures clearly demonstrate the lower $\mathbb{L}_2$ error of the tilted GBs with respect to the conventional ones for a wide range of collimation lengths and angles.

Fig. 5 plots the error vs. different observation line locations with respect to the collimation length, $0.2 < s_m/F_b < 1$, for $F = 40$, $k = 1e3[1/m]$ and for the three ϑ values 40°, 60° and 80°. The figure demonstrates that the tilted GB exhibits better accuracy within the localized beam domain, $s_m/F_b < 0.7$. Beyond the collimation-length, where the beam opens up, the tilted beams have no advantage over the conventional ones. Since beam-type expansions are generally used to take advantage of analytic simplicity which is introduced by the spatial and spectral localization of these waveobjects, these expansion schemes are tuned such that the GBs remains *well-collimated* within the domain of interest. The results in Fig. 5 clearly show that in the well-collimated regime, tilted GBs exhibit enhanced accuracy over the conventional ones. Full parameterization of different types of tilted GB waveobjects can be found in [50].

REFERENCES

[1] S. N. Vlasov and V. I. Talanov, "The parabolic equation in the theory of wave propagation," *Radiophys. Quantum Electron.*, vol. 38, pp. 1–12, 1995.
[2] M. Levys, *Parabolic Equation Methods for Electromagnetic Wave Propagation*. London, U.K.: Instit. Elect. Eng., 2000.
[3] C. Chapman, *Fundamentals of Seismic Wave Propagation*. Cambridge, UK: Cambridge Unive. Press, 2004.
[4] M. A. Leontovich and V. A. Fock, "Solution of the problem of EM wave propagation along the earth surface by the parabolic equation method," *J. Phys.*, vol. 10, p. 13, 1946.
[5] G. D. Malyuzhinets, "Progress in understanding diffraction phenomena (in russian)," *Sov. Phys. Usp.*, vol. 69, pp. 321–334, 1959.
[6] A. V. Popov, "Numerical solution of the wedge diffraction problem by the transversal diffusion method (in russian)," *Sov. Phys. Acoust.*, vol. 15, pp. 226–233, 1969.
[7] J. F. Claerbout, *Fundamentals of Geophysical Data Processing With Application to Petroleum Prospect*. New York: McGraw-Hill, 1976.
[8] F. D. Tappert, "The parabolic approximation method," in *Lecture Notes in Physics. Note 70, Wave Propagation and Underwater Acoustics*. New York: Springer Verlag, 1977, pp. 224–287.
[9] A. V. Popov and S. A. Hoziosky, "On a generalized parabolic equation of diffraction theory," (in Russian) *J. Comp. Math. Phys.*, vol. 17, pp. 527–533, 1977.
[10] V. M. Babič and V. S. Buldyrev, *Short-Wavelength Diffraction Theory*. New York: Spring-Verlag, 1990.
[11] V. A. Baranov and A. V. Popov, "Generalization of the parabolic equation for EM waves in a dielectric layer of nonuniform thickness," *Wave Motion*, vol. 17, pp. 337–347, 1993.
[12] A. E. Barrios, "A terrain parabolic equation model for propagation in the troposphere," *IEEE Trans. Antennas Propag.*, vol. 42, pp. 90–98, 1994.
[13] J. R. Kuttler, "Differences between the narrow-angle and wide-angle propagators in the split-step Fourier solution of the parabolic wave equation," *IEEE Trans. Antennas Propag.*, vol. 47, pp. 1131–1140, 1999.
[14] D. J. Donohue and J. R. Kuttler, "Propagation modeling over terrian using the parabolic wave equation," *IEEE Trans. Antennas Propag.*, vol. 48, pp. 260–277, 2000.
[15] A. E. Barrios, "Ray-tracing and parabolic equation methods in the modeling of a tropospheric microwave link," *IEEE Trans. Antennas Propag.*, vol. 53, pp. 3785–3791, 2005.
[16] R. D. Graglia, G. Guarnieri, G. Pelosi, and S. Seller, "The parabolic equation method for the high-frequency scattering from a convex perfectly conducting wedge with curved faces," *J. Electromag. Waves Appl.*, vol. 21, pp. 585–598, 2007.
[17] R. Martelly and R. Janaswamy, "An ADI-PE approach for modeling radio transmission loss in tunnels," *IEEE Trans. Antennas Propag.*, vol. 57, pp. 1759–1770, 2009.
[18] J. A. Arnaud and H. Kogelnik, "Gaussian light beams with general astigmatism," *Appl. Opt.*, vol. 8, pp. 1687–1693, 1969.
[19] G. A. Deschamps, "Gaussian beam as a bundle of complex rays," *Electron. Lett.*, vol. 7, pp. 684–685, 1971.
[20] E. G. Abramochkin and V. G. Volostnikov, "Spiral light beams," *Physics-Uspekhi*, vol. 47, pp. 1177–1203, 2004.

[21] S. Patil, M. Takale, V. Fulari, and M. Dongare, "Propagation of Hermite-cosh-Gaussian laser beams in non-degenerate Germanium having space charge neutrality," *J. Mod. Opt.*, vol. 55, pp. 3527–3533, 2008.
[22] M. V. Takale, S. T. Navare, S. D. Patil, V. J. Fulari, and M. B. Dongare, "Self-focusing and defocusing of TEM0p Hermite-Gaussian laser beams in collisionless plasma," *Opt. Commun.*, vol. 282, pp. 3157–3162, 2009.
[23] S. D. Patil, S. T. Navare, M. V. Takale, and M. B. Dongare, "Self-focusing of cosh-Gaussian laser beams in a parabolic medium with linear absorption," *Opt. Lasers Eng.*, vol. 47, pp. 604–606, 2009.
[24] V. Ĉerveny, M. M. Popov, and I. Pŝenĉik, "Computation of wave fields in inhomogeneous media—Gaussian beam approach," *Geophys. J. Roy. Asro. Soc*, vol. 70, pp. 109–128, 1982.
[25] E. Heyman, "Pulsed beam propagation in an inhomogeneous medium," *IEEE Trans. Antennas Propag.*, vol. 42, pp. 311–319, 1994.
[26] T. Melamed, "Phase-space Green's functions for modeling time-harmonic scattering from smooth inhomogeneous objects," *J. Math. Phys.*, vol. 46, pp. 2232–2246, 2004.
[27] S. Y. Shin and L. B. Felsen, "Gaussian beams in anisotropic media," *Appl. Phys.*, vol. 5, pp. 239–250, 1974.
[28] R. Simon, "Anisotropic Gaussian beams," *Opt. Commun.*, vol. 46, pp. 265–269, 1983.
[29] I. Tinkelman and T. Melamed, "Gaussian beam propagation in generic anisotropic wavenumber profiles," *Opt. Lett.*, vol. 28, pp. 1081–1083, 2003.
[30] I. Tinkelman and T. Melamed, "Local spectrum analysis of field propagation in anisotropic media, part I—Time-harmonic fields," *J. Opt. Soc. Am. A*, vol. 22, pp. 1200–1207, 2005.
[31] I. Tinkelman and T. Melamed, "Local spectrum analysis of field propagation in anisotropic media, part II—Time-dependent fields," *J. Opt. Soc. Am. A*, vol. 22, pp. 1208–1215, 2005.
[32] A. G. Khatkevich, "Propagation of pulses and wave packets in dispersive gyrotropic crystals," *J. Appl. Spectrosc.*, vol. 46, pp. 203–207, 1987.
[33] T. Melamed and L. B. Felsen, "Pulsed beam propagation in lossless dispersive media, part I: Theory," *J. Opt. Soc. Am. A*, vol. 15, pp. 1268–1276, 1998.
[34] T. Melamed and L. B. Felsen, "Pulsed beam propagation in lossless dispersive media, part II: A numerical example," *J. Opt. Soc. Am. A*, vol. 15, pp. 1277–1284, 1998.
[35] T. Melamed and L. B. Felsen, "Pulsed beam propagation in dispersive media via pulsed plane wave spectral decomposition," *IEEE Trans. Antennas Propag.*, vol. 48, no. 6, pp. 901–908, 2000.
[36] A. P. Kiselev, "Localized light waves: Paraxial and exact solutions of the wave equation (a review)," *Opt. Spectrosc.*, vol. 102, pp. 603–622, 2007.
[37] J. J. Maciel and L. B. Felsen, "Systematic study of fields due to extended apertures by Gaussian beam discretization," *IEEE Trans. Antennas Propag.*, vol. 37, pp. 884–892, 1989.
[38] B. Z. Steinberg, E. Heyman, and L. B. Felsen, "Phase space beam summation for time-harmonic radiation from large apertures," *J. Opt. Soc. Am. A*, vol. 8, pp. 41–59, 1991.
[39] A. Shlivinski, E. Heyman, A. Boag, and C. Letrou, "A phase-space beam summation formulation for ultra wideband radiation," *IEEE Trans. Antennas Propag.*, vol. 52, pp. 2042–2056, 2004.
[40] A. Shlivinski, E. Heyman, and A. Boag, "A pulsed beam summation formulation for short pulse radiation based on windowed radon transform (WRT) frames," *IEEE Trans. Antennas Propag.*, vol. 53, pp. 3030–3048, 2005.
[41] B. Z. Steinberg, E. Heyman, and L. B. Felsen, "Phase space beam summation for time dependent radiation from large apertures: Continuous parametrization," *J. Opt. Soc. Am. A*, vol. 8, pp. 943–958, 1991.
[42] T. Melamed, "Phase-space beam summation: A local spectrum analysis for time-dependent radiation," *J. Electromag. Waves Appl.*, vol. 11, pp. 739–773, 1997.
[43] T. Melamed, "Exact beam decomposition of time-harmonic electromagnetic waves," *J. Electromag. Waves Appl.*, vol. 23, pp. 975–986, 2009.
[44] L. A. Stratton, *Electromagnetic Theory*. New York: McGraw-Hill, 1941.
[45] E. Heyman and T. Melamed, "Certain considerations in aperture synthesis of ultrawideband/short-pulse radiation," *IEEE Trans. Antennas Propag.*, vol. 42, pp. 518–525, 1994.
[46] E. Heyman and T. Melamed, *Space-Time Representation of Ultra Wideband Signals*. The Netherlands: Elsevier, 1998, vol. 103, Advances in Imaging and Electron Physics, pp. 1–63.
[47] H.-T. Chou, P. H. Pathak, and R. J. Burkholder, "Application of Gaussian-ray basis functions for the rapid analysis of electromagnetic radiation from reflector antennas," *Proc. Inst. Elect. Eng. Microw. Antennas Propag.*, vol. 150, pp. 177–183, 2003.
[48] H.-T. Chou, P. H. Pathak, and R. J. Burkholder, "Novel Gaussian beam method for the rapid analysis of large reflector antennas," *IEEE Trans. Antennas Propag.*, vol. 49, pp. 880–893, 2001.
[49] H.-T. Chou and P. H. Pathak, "Fast Gaussian beam based synthesis of shaped reflector antennas for contoured beam applications," *IEE Proc., Microw. Antennas Propag.*, vol. 151, pp. 13–20, 2004.
[50] Y. Hadad and T. Melamed, "Parameterization of the tilted Gaussian beam waveobjects," *Progr. Electromagn. Res., PIER*, vol. 102, pp. 65–80, 2010.

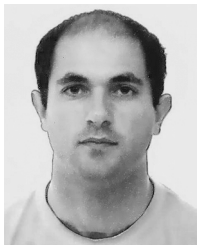

Yakir Hadad was born in Beer Sheva, Israel, in 1984. He received the B.Sc. (*summa cum laude*) and M.Sc. (*summa cum laude*) degrees in electrical and computer engineering from Ben-Gurion University of the Negev, Israel, in 2005 and 2008, respectively.

Currently, he is a Ph.D. student in the Department of Physical-Electronics, School of Electrical Engineering, Tel-Aviv University, Israel. His main fields of interest are asymptotic methods, artificial materials and analytic modeling in electromagnetics.

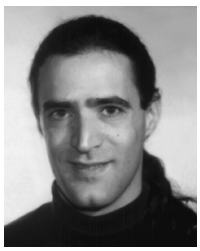

Timor Melamed was born is Tel-Aviv, Israel, in January 1964. He received the B.Sc. degree (*magna cum laude*) in electrical engineering in 1989 and the Ph.D. degree in 1997, both from Tel-Aviv University, Israel.

From 1996 to 1998, he held a postdoctoral position at the Department of Aerospace and Mechanical Engineering, Boston University, Boston, MA. From 1999 to 2000, he was with Odin Medical Technologies. Currently he is with the Department of Electrical and Computer Engineering, Ben Gurion University of the Negev, Israel. His main fields of interest are analytic techniques in wave theory, transient wave phenomena, inverse scattering and relativistic electrodynamics.